ACS APPLIED MATERIALS & INTERFACES

Research Article

www.acsami.org

Facile Preparation of Ultra-Large Pore Mesoporous Silica Nanoparticles and Their Application to the Encapsulation of Large Guest Molecules

Hye-Seon Shin, Yong-Kyung Hwang, and Seong Huh*

Department of Chemistry and Protein Research Center for Bio-Industry, Hankuk University of Foreign Studies, Yongin 449-791, Korea

ABSTRACT: Pore-enlarged mesoporous silica nanoparticles (MSNs) were prepared directly from as-prepared MSNs through a new, simple method using divalent Ca or Mg salts as both efficient silica etching reagents and as ion exchangers in methanolic solution under mild conditions. The resultant MSNs became almost template-free simultaneously during this etching process. The pore-enlarged MSNs, referred to as Ca-MSN or Mg-MSN, maintained their original hexagonal pore symmetry and particle sizes, but several ultra-large mesopores were generated inside and outside the MSNs together with regular mesopores having expanded pore dimension of around 4−5 nm. The average pore diameters for ultra-large pores were 47.5 nm for Ca-MSN and 52.4 nm for Mg-MSN. The generation of ultra-large pores can be regarded as the collapse of several mesopores into an ultra-large pore. Both Ca-MSN and Mg-MSN were good sorbents for positively charged porphyrin molecules. Additionally, these ultra-large pore MSNs exhibited better adsorption ability than calcined MSN for large proteins and antibodies, such as bovine serum albumin (BSA) and immunoglobulin G (IgG).

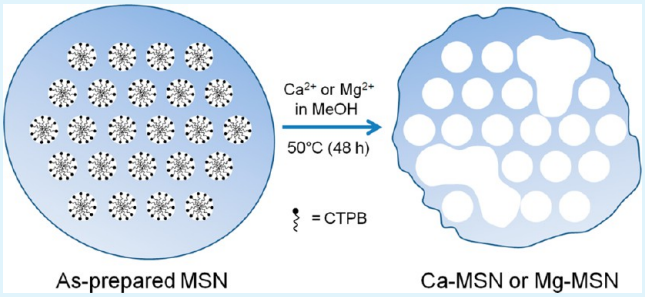

KEYWORDS: *mesoporous silica nanoparticles, large pore mesoporous silicas, silica etching, protein sequestration, porphyrin encapsulation, drug delivery*

INTRODUCTION

Mesoporous silica nanoparticles (MSNs) have been intensively employed as efficient drug or protein delivery carriers because of their large surface area and pore volume of ordered mesoscale pores for a wide range of guests, from small molecules to proteins.[1] The high internalization efficacy of MSN into various cells via endocytosis may also have great advantages over other competing carriers.[2−5] There is an increasing number of publications relevant to controlled-release systems based on MSNs by sophisticated capping and uncapping methods of guest loaded mesopores.[6−10] However, one critical drawback of MSN delivery systems for large guest molecules such as proteins is the limited pore dimension of mesopores, which usually ranges from 2 to 5 nm.[11,12] The original method for pore expansion of MCM-41 by Kresge et al. involves the use of a hydrophobic pore expander molecule, which is also called a swelling agent.[13] For instance, by simply adding varying amounts of 1,3,5-trimethylbenzene (TMB) as a pore expander into MCM-41 precursor solution, pore-expanded MCM-41 with pore dimensions up to 6.5 nm has been successfully obtained. Zhao et al. developed a method of using a nonionic pluronic-based template system for SBA-15 to overcome the weak framework stability of a siliceous wall under hydrolytic conditions.[14,15] SBA-15 indeed exhibited large mesopores as well as a thicker silica wall than MCM-41. Furthermore, by simply changing the aging temperature of a silica sol containing P123 block copolymer, the pore dimensions of SBA-15 were finely tuned up to 8.9 nm. However, these methods still have limited usage for pore expansion of sub-200 nm MSNs.

Very recently, researchers have made attempts to overcome this issue. Several promising reports provided MSNs with expanded mesopores. Min and Ryoo et al. reported MSNs with expanded pores obtained using a two-step synthetic method.[16,17] They firstly prepared MSNs and then thermally treated the acid-extracted MSNs in the presence of an excess amount of TMB with an equal volume of ethanol at 140 °C for 4 days. The final pore-expanded MSN exhibited pore dimensions of 23 nm. Despite the successful application of the pore-expanded MSNs to gene delivery, the preparation method requires a long reaction period and high-temperature heat treatment in a high-pressure bomb. Thus, a new, simple method to prepare pore-enlarged MSN is highly desirable for various advanced applications. In this report, we demonstrate an efficient preparation method for pore-enlarged MSNs under very mild conditions with a short period of reaction and without significant changes in particle size.

Received: October 24, 2013
Accepted: January 21, 2014
Published: January 21, 2014

To prepare MSN materials with ultra-large pore dimensions, we adopted a selective etching approach instead of more commonly used methods using pore expander molecules. It is well known that zeolitic aluminosilicate can be selectively etched to produce pore-enlarged aluminosilicate through partial demetallation processes, such as dealumination or desilication.[18−20] In these processes, Al or Si atoms can be selectively removed by steam or chemical etchants, and the pore dimensions are consequently increased partially. We envisioned that the controlled etching of SiO_2 in sub-200 nm MSNs would produce pore-enlarged MSN materials. The MSN size can be kept at sub-200 nm, which is apt for various advanced applications.

EXPERIMENTAL DETAILS

Preparation of MSN. MSN was prepared by using cetylpyridinium bromide (CTPB) as a surfactant and tetraethyl orthosilicate (TEOS) as a silica source in basic medium. CTPB (1.050 g, 2.73 mmol) and 2.0 M NaOH aqueous solution (3.5 mL) were mixed in deionized water (240 mL) at 80 °C for 40 min, and a transparent yellow color was developed immediately. TEOS (5.0 mL, 22.4 mmol) was injected into the mixture quickly and stirred at 80 °C for an additional 2.5 h. The resultant yellow solids were filtered and washed with a copious amount of deionized water, and then dried overnight at 80 °C. Surfactant templates were removed by calcination in air at 550 °C for 5 h.

Preparation of Ca-MSN. As-prepared MSN solid (0.5 g) was mixed with $Ca(NO_3)_2{\cdot}4H_2O$ solution (100 mL, 0.1 M dissolved into methanol) and then stirred at 50 °C for 48 h. Hot filtered precipitates were washed with methanol and deionized water, then dried at 80 °C overnight.

Preparation of Mg-MSN. Mg-MSN was prepared using the similar synthetic method of Ca-MSN. As-prepared MSN solid (0.5 g) was mixed with $Mg(NO_3)_2{\cdot}6H_2O$ solution (100 mL, 0.1 M dissolved into methanol) and stirred at 50 °C for 48 h. Hot filtered precipitates were washed with methanol and deionized water several times, and dried at 80 °C overnight.

Experiment of Porphyrin Immobilization. Three porphyrin compounds, meso-tetra(4-*N*-methylpyridyl)porphine tetraiodide (TMPYP, Strem), meso-tetraphenyl-21*H*,23*H*-porphine zinc (ZnTPP, Sigma-Aldrich), and tetrasodium meso-tetra(4-sulfonatephenyl)porphine dodecahydrate (TSPHP, Strem), with different charges, were exploited to identify the surface properties of each silica nanosphere. Silica nanoparticles (10 mg, MSN, Ca-MSN, and Mg-MSN, respectively) were mixed with 0.5 mM porphyrin solution (10 mL, dissolved into acetone for ZnTPP and deionized water for TMPYP and TSPHP, respectively) and stirred gently at room temperature in the dark for 24 h. The mixture was centrifuged at 9000 rpm for 15 min, and the supernatant was collected. To determine the residual amounts of porphyrin in the supernatant, 100-fold diluted supernatant was monitored by UV−vis spectrometry at the characteristic absorption wavelength of each porphyrin compound (TMPYP at 421 nm, ZnTPP at 421 nm, and TSPHP at 414 nm).

Experiment of Protein Immobilization. Two types of proteins, IgG from goat serum (Sigma no. I5256) and BSA (Sigma no. A2153), were used for immobilization experiments. IgG was adsorbed from PBS solution (pH 7.40) onto silica samples, and BSA adsorption was carried in acetate buffer solution (pH 4.80). Each silica sample (5 mg, MSN, Ca-MSN, Mg-MSN, respectively) was incubated in advance in a proper buffer solution (2.5 mL), that is, PBS for IgG adsorption and acetate buffer for BSA adsorption, for 1 h with gentle stirring. Protein solution (2.5 mL), dissolved into an appropriate buffer with a concentration of 0.8 mg mL^{-1}, was injected into the silica mixtures, and then stirred at room temperature for 24 h. The mixtures were centrifuged at 9000 rpm for 20 min, and the supernatants of each sample were collected. The residual protein concentrations of each supernatant were determined by Bradford assay (Sigma no. B6916) with the absorbance at 595 nm.

Physical Measurements. Powder X-ray diffraction patterns were recorded on a Bruker D8 Advance diffractometer (40 kV, 40 mA, step size = 0.02°). FE-SEM images were recorded on a Hitachi Ultra-High-Resolution Analytical FE-SEM SU-70 (accelerating voltage = 5 kV). The acetone suspension of the sample was dropped and dried on a Cu grid supported by carbon film for TEM measurement, for which a JEOL JEM-3000F (300 kV) equipped with an EDAX for EDS spectrum was used. Electron tomography was performed on a Tecnai G2 Spirit (120 kV) at the Korea Basic Science Institute. Raw data were obtained from +60° to −60° every 2°. Image alignment was done using IMOD software. Rendered images were obtained by AMIRA 4.0 software. Solid-state magic-angle spinning (MAS) nuclear magnetic resonance (NMR) spectra were taken on a Bruker Avance II spectrometer at frequencies of 99.4, 125.8, and 500 MHz for ^{29}Si, ^{13}C, and ^{1}H nuclei, respectively. ^{29}Si and ^{13}C nuclei were observed using direct-polarization (DP) or by cross-polarization (CP) from the neighboring ^{1}H nuclei. ^{29}Si DP-MAS spectra were calibrated using tetramethylsilane (TMS). Sample rotors were rotated at a spinning rate of 5 kHz. The ζ-potential measurement was performed by an Otsuka ELS-8000 electrophoretic light scattering spectrophotometer. Sample particles (3 mg) were suspended in distilled water (10 mL), sonicated for 30 min, and the ζ-potential was measured. The N_2 adsorption-desorption analysis was performed on a Belsorp-miniII at 77 K (BEL Japan). Hg-porosimetric analyses were performed on a Micromeritics AutoPore IV 9500. The samples were dried at 423 K under high vacuum for 2 h. The carbon contents of the samples were analyzed using an EA1112 (CE Instruments, Italy).

RESULTS AND DISCUSSION

Conventional MSN material was prepared by a modified method from the literature,[21,22] using cetylpyridinium bromide (CTPB) in a basic solution. The average particle size of the MSNs was less than 200 nm, which was estimated from TEM images as in Figure 1. Sphere and rod particle morphologies

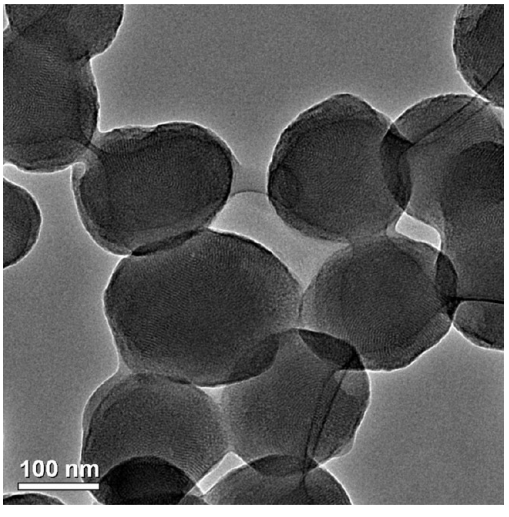

Figure 1. TEM image of calcined MSN.

were observed. To remove the CTPB template through ion exchange, the as-prepared MSN was treated with 0.1 M methanolic solutions of $Ca(NO_3)_2{\cdot}4H_2O$ or $Mg(NO_3)_2{\cdot}6H_2O$ at 50 °C for 48 h. The resulting samples are denoted as Ca-MSN and Mg-MSN, respectively.

The particle morphology of the calcined MSN and Ca-MSN were investigated by scanning electron microscopy (SEM) to find any discrepancies between the two samples. Unlike calcined MSN (Figure 2a), Ca-MSN exhibited very rough particle surfaces, as depicted in Figure 2b. The entire particles

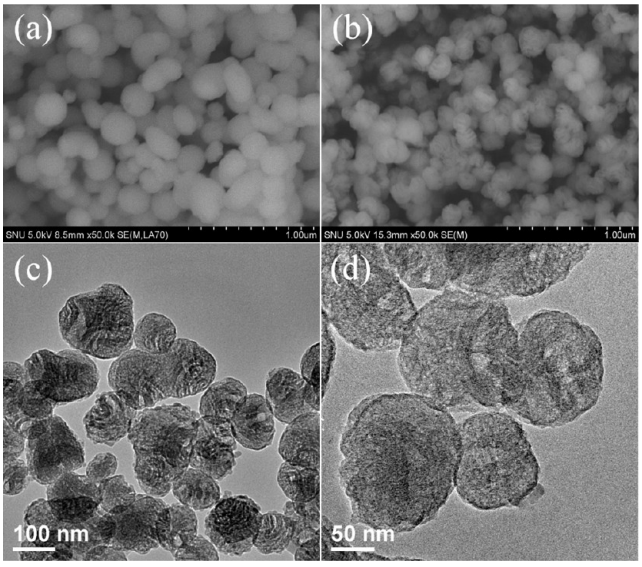

Figure 2. FE-SEM images of calcined MSN (a) and Ca-MSN (b). Both images were taken on the same magnification without metallic coating (×50 000). TEM images of Ca-MSN (c) and Mg-MSN (d) on different magnifications.

keep their original sizes, but very large channels and surface defects can clearly be seen in the SEM image. Transmission electron microscopy (TEM) investigation clearly revealed the large channels generated for Ca-MSN, as shown in Figure 2c. Overall, the particle size did not change significantly, but there were very large new channels. Thus, the treatment of 0.1 M methanolic solution of $Ca(NO_3)_2{\cdot}4H_2O$ could efficiently generate very large channels for Ca-MSN.

The residual amount of CTPB template in Ca-MSN was also estimated by solid-state ^{13}C cross-polarization magic angle spinning (CP-MAS) NMR spectroscopy. Surprisingly, there was a very small amount of residual CTPB template, according to the very weak magnetic resonance signals of CTPB obtained with an extended acquisition period (5 h), compared with those of the as-prepared MSNs acquired for 3 h as depicted in Figure 3. None of the aromatic signals of CTPB at 144.8 and 128.8 ppm were observed for both Ca-MSN and Mg-MSN. In addition, elemental analysis revealed that the carbon content in Ca-MSN was merely 2.8 wt %, while the carbon content in the as-prepared MSN was 31.7 wt %.

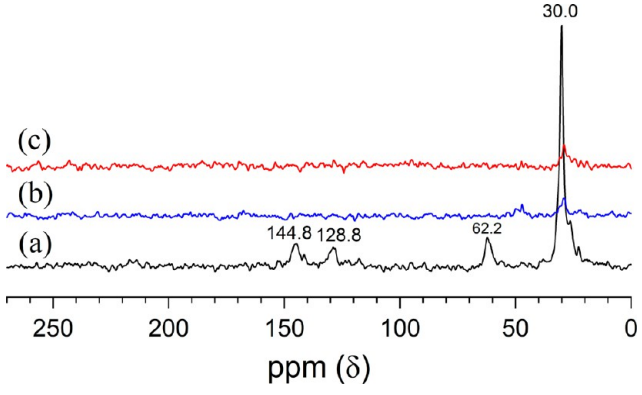

Figure 3. Solid-state ^{13}C CP-MAS NMR spectra for as-prepared MSN (a), Ca-MSN (b), and Mg-MSN (c). Characteristic signals from CTPB are indicated in panel a.

Thermogravimetric analysis (TGA) indicated that the residual amount of CTPB in Ca-MSN was very small relative to the as-prepared MSNs as in Figure 4. After initial weight loss at about 120 °C because of the removal of surface captured water molecules, the final weight loss at 800 °C was less than 5 wt %.

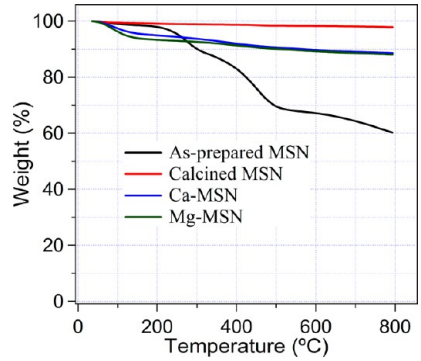

Figure 4. TG profiles for the as-prepared MSN, calcined MSN, Ca-MSN, and Mg-MSN.

On the basis of these results, we concluded that the treatment with $Ca(NO_3)_2{\cdot}4H_2O$ methanolic solution was effective at both removing the CTPB template through either the simple ion-exchange of CTP^+ ions with Ca^{2+} ions or protons, or the etching of the silica wall by Ca^{2+} ions to produce large channels (Scheme 1). At present, the etching

Scheme 1. Illustration of the Generation of Template-Free Ca-MSN and Mg-MSN through the Framework Etching and Ion-Exchange of CTPB Template

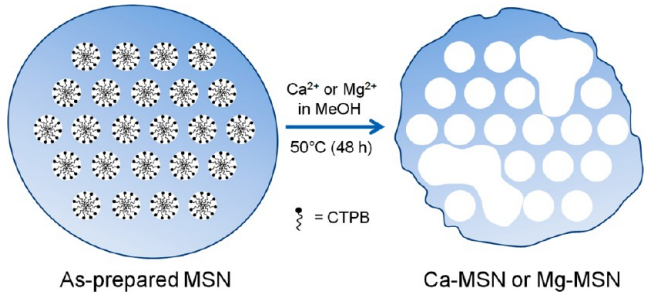

mechanism of silica by Ca^{2+} ions is thought to be a combined result of the acidic 0.1 M methanolic solution of $Ca(NO_3)_2{\cdot}4H_2O$ (pH ~ 5.65) and the direct attack of Ca^{2+} ions onto SiO_2. Interestingly, $Mg(NO_3)_2{\cdot}6H_2O$ treatment gave a very similar result to that of $Ca(NO_3)_2{\cdot}4H_2O$ treatment. The measured pH value of 5.32 for the 0.1 M methanolic solution of $Mg(NO_3)_2{\cdot}6H_2O$ was also acidic. Mg-MSN also displayed rough etched surface texture (Figure 5). The TEM image shown in Figure 2d revealed both new enlarged mesopores and original mesopores templated from the CTPB. However, by careful examination of the SEM and TEM images, the etching efficiency using $Ca(NO_3)_2{\cdot}4H_2O$ solution seems to be more effective than using $Mg(NO_3)_2{\cdot}6H_2O$ solution under the same conditions. Although Yu and co-workers previously reported mesoporous silica preparation method of adding NaCl and NH_4Cl salts in the reaction mixture,[23] the etching method using alkaline earth metal salts for as-prepared MSNs described in this study has not been reported.

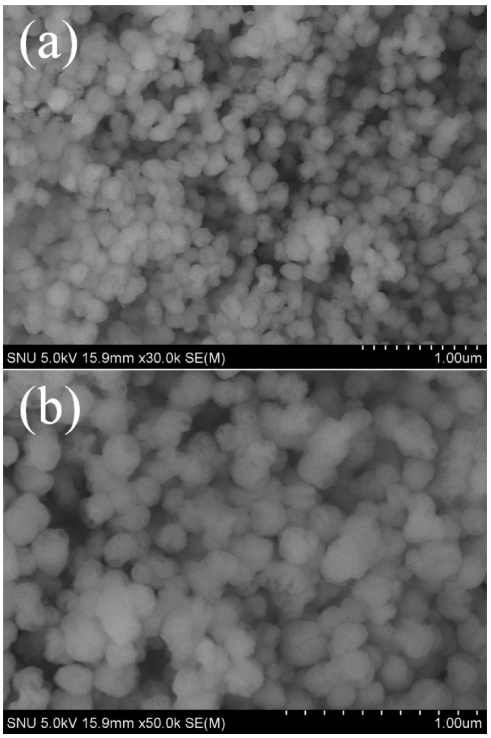

Figure 5. SEM images of non-coated Mg-MSN on different magnifications: ×30 000 (a) and ×50 000 (b).

Both samples exhibited very similar powder X-ray diffraction (PXRD) patterns compared with the pattern of calcined MSN (Figure 6a). Thus, the frameworks of Ca-MSN and Mg-MSN

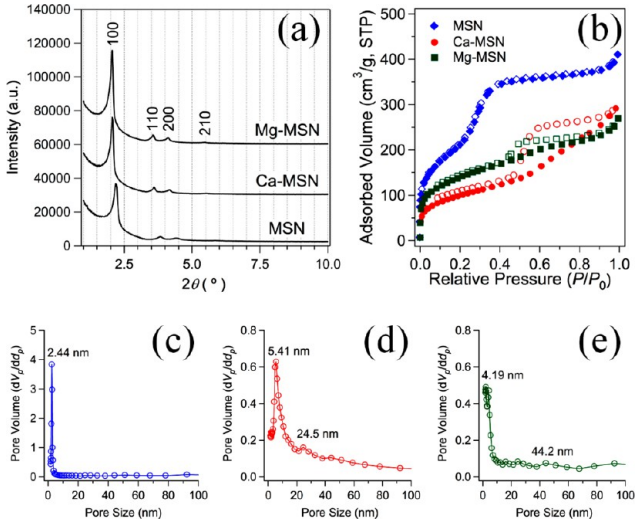

Figure 6. PXRD patterns of calcined MSN, Ca-MSN, and Mg-MSN (a). N_2 gas adsorption/desorption isotherms for MSN, Ca-MSN, and Mg-MSN (b). BJH pore size distribution curves for MSN (c), Ca-MSN (d), and Mg-MSN (e).

maintain the hexagonal symmetry of the MSNs with the well-resolved diffraction patterns characteristic of hexagonal MCM-41 silicas including (100), (110), (200), and (210) peaks with the spacing ratio of $1:\sqrt{3}:\sqrt{4}:\sqrt{7}$.[21,22] The diffraction peaks indexed as (100) plane for both Ca-MSN (2.06°, *d*-spacing = 4.29 nm) and Mg-MSN (2.06°, *d*-spacing = 4.29 nm) exhibited very slight change compared with that of calcined MSN observed at 2.19° (*d*-spacing = 4.03 nm). Despite the pore enlargement, the unitcell dimension of hexagonal mesopores remained almost constant. We could not observe the peaks responsible for ultra-large pores presumably because of their large dimension or small number of diffraction planes. Both Ca-MSN (312 $m^2\ g^{-1}$) and Mg-MSN (425 $m^2\ g^{-1}$) displayed substantial decreases in Brunauer–Emmett–Teller (BET) surface areas compared with calcined MSN (760 $m^2\ g^{-1}$) (Figure 6b). This can be accounted for by pore enlargement. Unexpectedly, the pore volume of 0.63 $cm^3\ g^{-1}$ for MSNs was also larger than those of Ca-MSN (0.45 $cm^3\ g^{-1}$) and Mg-MSN (0.41 $cm^3\ g^{-1}$). The decreased pore volumes of Ca-MSN and Mg-MSN compared with calcined MSN are mainly due to the simultaneous etching of exterior surfaces of Ca-MSN and Mg-MSN which cannot increase pore volume significantly. Barrett–Joyner–Halenda (BJH) pore size distribution curves further support the presences of ultra-large pores as well as expanded mesopores (Figure 6c–6e). The original mesopore with a dimension of 2.44 nm for MSN was expanded to 5.41 nm for Ca-MSN and 4.19 nm for Mg-MSN. Pore dimensions of 24.5 and 44.2 nm for ultra-large pores were also observed. Additionally, the average pore diameters ($4V_{tot}/A_{tot}$) of ultra-large pores were estimated by Hg-porosimetry where V_{tot} is total intrusion volume and A_{tot} is total pore area. Ca-MSN and Mg-MSN displayed average pore diameters of 47.5 and 52.4 nm, respectively. These values agree well with the values estimated from TEM analysis. Traditionally, an acid-extraction process is commonly employed for the removal of ammonium-based organic templates in the as-prepared MSN with organic functionalities on its surface.[24,25] In this case, however, the severe etching of the silica framework was not observed. As a result, the acid-extracted sample usually exhibited well-ordered hexagonal channels with a large surface area. Alternatively, the treatment of silica materials with basic aqueous hydroxide solution is also known to be effective for silica etching to produce different types of porous materials, including porous hollow silica spheres,[26] silica@carbon core/shell particles,[27] Au@silica core/shell nanospheres,[28] and corrugated porous silica spheres.[29] However, none of these methods gave the same results as those in the current report. Thus, the etching method of using alkaline earth metal salts as an etchant is a new and attractive approach for obtaining pore-enlarged MSNs.

TEM image of ultramicrotomed Ca-MSN also clearly indicates that the new large channels are located inside the Ca-MSN, as well as on the surface (Figure 7). To investigate the pore texture of Ca-MSN in detail, three-dimensional (3D) TEM tomography was employed. We can obtain the 3D morphology of the particle by constructing individual 2D TEM images over different tilting angles with a single Ca-MSN (Figure 8). Figure 9 shows reconstructed TEM tomography images of the Ca-MSN. The Ca-MSN in Figure 9a is a normal TEM image for comparison. A cross-sectional image (Figure 9b) taken from the 3D reconstruction of a Ca-MSN clearly shows two ultra-large mesopores (light-gray regions) penetrating from one end to the other, which could be suitable for entrapping large guest molecules. The pore dimensions of the two pores are about 43.8 and 32.9 nm based on the longest diameter. Completely reconstructed 3D volume images (Figure 9c and 9d) reveal several openings of ultra-large mesopores on the surface.

The zeta potentials (ζ-potential) of Ca-MSN and Mg-MSN were measured for surface characterization (Table 1).[30] Both Ca-MSN (−23.60 mV) and Mg-MSN (−21.50 mV) have

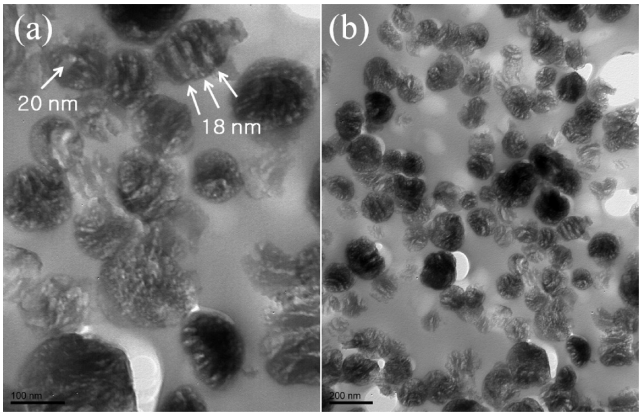

Figure 7. TEM images of microtomed Ca-MSN which was embedded in epoxy resin on different magnifications (a, b). Well-defined canals and surface texture are clearly seen in most Ca-MSNs. Arrows in (a) indicate representative ultra-large mesopores developed inside Ca-MSNs and whose dimensions are about 18 nm and 20 nm.

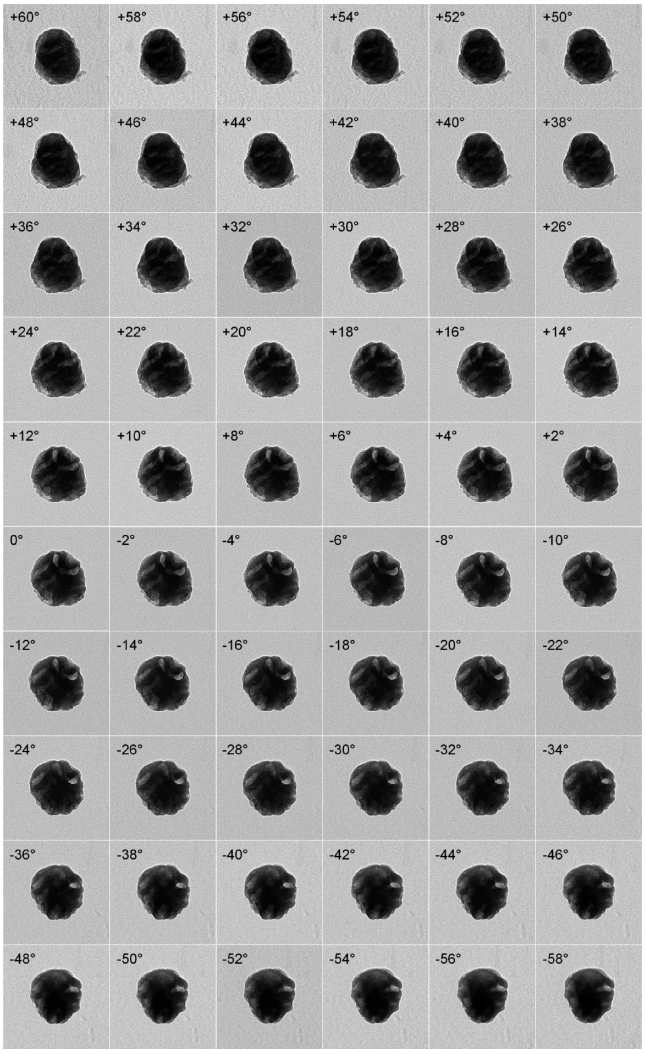

Figure 8. TEM images of a Ca-MSN collected on different tilting angles.

relatively smaller values of surface potential compared with calcined MSN (−36.66 mV). This can be regarded to mainly be due to residual cations on their surfaces. However, it was also

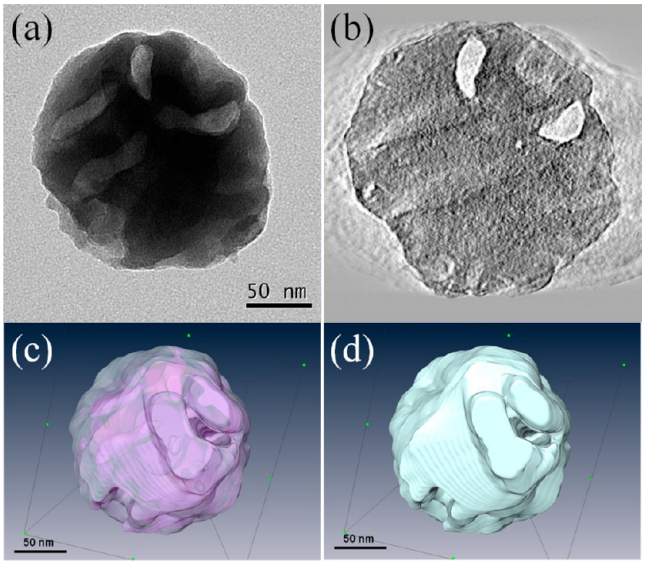

Figure 9. 2D TEM image of Ca-MSN (a) and its cross-sectioned image (b) taken from 3D reconstruction of a single Ca-MSN. The sliced image depicts the existence of large channels through the spheres (light gray color). 3D reconstructed images of tomogram are shown in panels c and d.

Table 1. ζ-Potential for MSN, Ca-MSN, and Mg-MSN

materials	ζ-potential [mV]
calcined MSN	−36.66 ± 0.46
Ca-MSN	−23.60 ± 0.39
Mg-MSN	−21.50 ± 0.43

revealed that only small amounts of cations remained, based on the inductively coupled plasma (ICP) analysis, with 1.94 wt % of Ca in Ca-MSN and 1.35 wt % of Mg in Mg-MSN. Because the contents of residual Ca or Mg ions on surfaces are relatively small, the reduced surface charges for Ca-MSN and Mg-MSN could be attributed to higher condensation extent of acidic surface silanol (Si−OH) groups. This can be clearly supported by solid-state ^{29}Si DP-MAS NMR spectra in Figure 10. Analysis of the three MSNs by solid-state ^{29}Si DP-MAS NMR offered information on the degree of condensation of silica frameworks. The silicon resonance peaks representing Q^4 ($(\equiv SiO)_4\mathbf{Si}$), Q^3 ($(\equiv SiO)_3\mathbf{Si}OH$), and Q^2 ($(\equiv SiO)_2\mathbf{Si}(OH)_2$) were observed in their characteristic positions.[21] The ratio, $Q^4/(Q^3 + Q^2)$, is a quantitative assessment of degree of condensation of silica framework. As expected, the ratios for Ca-MSN (2.03) and Mg-MSN (1.70) are much larger than calcined MSN (1.17). Therefore, the decreases of surface charge for Ca-MSN and Mg-MSN can be attributed to further condensation of silica frameworks during alkaline earth metal salt treatment.

Three porphyrin compounds with different charges were used for the adsorption test for large guest molecules, as depicted in Figure 11a. We chose a series of porphyrin molecules, because porphyrins encapsulated in MSN could be utilized for various applications such as catalysis,[31] photosensitization,[32] and potential cancer theranostics.[33] Meso-tetra(4-*N*-methylpyridyl)porphine tetraiodide (TMPYP) and tetrasodium meso-tetra(4-sulfonatephenyl)porphine dodecahydrate (TSPHP) have permanent positive and negative charges, respectively, and meso-tetraphenyl-21*H*,23*H*-porphine zinc (ZnTPP) is neutral. As given in Figure 11b, positively charged TMPYP species are adsorbed the most, and adsorptions of

dx.doi.org/10.1021/am404709w | ACS Appl. Mater. Interfaces 2014, 6, 1740−1746

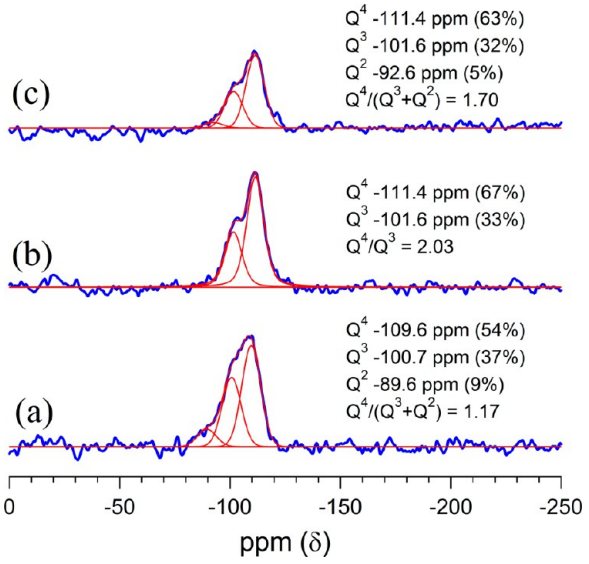

Figure 10. Deconvoluted solid-state ^{29}Si DP-MAS NMR spectra for calcined MSN (a), Ca-MSN (b), and Mg-MSN (c).

TSPHP with negative charges have the smallest values. It is notable that both Ca-MSN and Mg-MSN adsorbed more TMPYP than MSN despite their lower surface areas and negative charges, which clearly indicates high capacities for the encapsulation of both materials because of large pores than that of MSN. In addition, the adsorption amounts exceeded the previously reported value of 177 mg per gram for mesoporous silica with a BET surface area of 950 m^2 g^{-1} and a pore diameter of 3.5 nm.[34] However, despite the lower surface charges of Ca-MSN and Mg-MSN, both Ca-MSN and Mg-MSN exhibited lower adsorption amounts for the negatively charged guest, TSPHP, and neutral guest, ZnTPP, than MSN. Thus, ultra-large pore Ca-MSN and Mg-MSN are more effective at capturing positively charged guest molecules.

To study the biomolecular sequestration abilities of Ca-MSN and Mg-MSN, the uptake amounts of bovine serum albumin (BSA) and immunoglobulin G (IgG), which have large molecular size (69 and 150 kDa, respectively), were explored (Figure 11c). Both proteins could be used for the estimation of efficiency of large protein or antibody sequestration by porous materials.[11,12] The intracellular delivery of BSA and IgG by porous materials indicates limited success.[11,12,35] The adsorbed amounts of protein and antibody were estimated by Bradford assay. Approximately 307 mg of BSA and 262 mg of IgG were adsorbed onto a gram of Ca-MSN, and these values were higher than those on Mg-MSN (263 mg for BSA and 115 mg for IgG) and MSN (250 mg for BSA and 162 mg for IgG), as given in Figure 11d. The larger values of immobilization amounts on Ca-MSN than those of Mg-MSN are attributed to the well-developed ultra-large mesopore structures. Considering the lower surface area of Ca-MSN than calcined MSN, these higher adsorption capacities for BSA and IgG are impressive and important for protein delivery and enzyme immobilization. The Ca^{2+} ions on the silica surfaces can also enhance the adsorption of proteins and large molecules due to their high affinity.[36] We also explored the in vitro release of adsorbed IgG from Ca-MSN. The release profile indicates that the release kinetics is very slow at the beginning stage of release, and then gradually increases (Figure 11e). On the basis of these results, Ca-MSN is indeed a prospective carrier for large guest molecules.

CONCLUSION

We developed a new efficient synthesis method for ultra-large pore MSNs, Ca-MSN or Mg-MSN, by using divalent Ca or Mg salts as effective silica etching reagents. The as-prepared MSNs could also become template-free during the etching process. The synthesized Ca-MSN and Mg-MSN have unusually large channels that can accommodate large proteins and antibodies, as well as positively charged porphyrin inside the enlarged pores. Although both Ca-MSN and Mg-MSN exhibited lower surface areas than the calcined MSN due to the generation of large mesopores, their BSA loading capacities were slightly higher than that of the calcined MSN. In the case of IgG adsorption, Ca-MSN exhibited higher adsorption capacity than MSN, while Mg-MSN showed lower adsorption capacity than MSN. The pore-enlarged MSN would be useful for intracellular

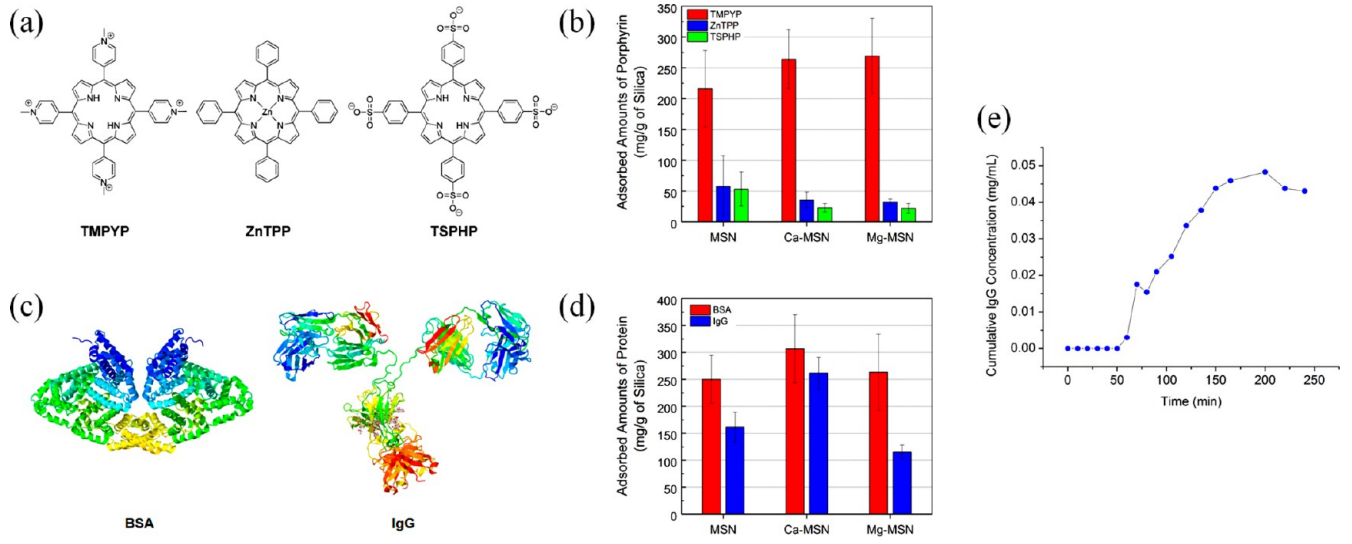

Figure 11. Structures of three porphyrin guest molecules (a). Adsorbed amounts of three porphyrin compounds onto MSN, Ca-MSN, and Mg-MSN (b). Structures of BSA (PDB entry 4F5S) and IgG (PDB entry 1IGT) (c). Adsorbed amounts of BSA and IgG onto MSN, Ca-MSN, and Mg-MSN (d). Each adsorption experiment was performed in triplicate. IgG release profile of Ca-MSN containing IgG (e).

delivery and the immobilization of large proteins. Furthermore, our new findings will lead to a new methodology for the preparation of ultra-large pore inorganic porous materials for diverse advanced applications.

AUTHOR INFORMATION

Corresponding Author

*E-mail: shuh@hufs.ac.kr.

Author Contributions

The manuscript was written through contributions of all authors. All authors have given approval to the final version of the manuscript. Hye-Seon Shin and Yong-Kyung Hwang contributed equally.

Notes

The authors declare no competing financial interest.

ACKNOWLEDGMENTS

This work was supported by the Basic Science Research Program through the National Research Foundation of Korea (NRF) funded by the Ministry of Education, Science and Technology (2013R1A1A2006914), and the Gyeonggi Regional Research Center (GRRC) Program of Gyeonggi Province (GRRC-HUFS-2013-B04).

ABBREVIATIONS

MSN, mesoporous silica nanoparticle
CTPB, cetylpyridinium bromide
TEM, transmission electron microscopy
SEM, scanning electron microscopy
PXRD, powder X-ray diffraction
BET, Brunauer-Emmett-Teller
BJH, Barrett-Joyner-Halenda
CP-MAS, cross-polarization magic-angle spinning
DP-MAS, direct-polarization magic-angle spinning
NMR, nuclear magnetic resonance
TGA, thermogravimetric analysis
ICP, inductively coupled plasma
TMPYP, meso-tetra(4-*N*-methylpyridyl)porphine tetraiodide
TSPHP, tetrasodium meso-tetra(4-sulfonatephenyl)-porphine dodecahydrate
ZnTPP, meso-tetraphenyl-21*H*,23*H*-porphine zinc
BSA, bovine serum albumin
IgG, immunoglobulin G

REFERENCES

(1) Tang, F.; Li, L.; Chen, D. *Adv. Mater.* **2012**, *24*, 1504−1534.
(2) Slowing, I. I.; Vivero-Escoto, J. L.; Wu, C.-W.; Lin, V. S.-Y. *Adv. Drug Delivery Rev.* **2008**, *60*, 1278−1288.
(3) Rosenholm, J. M.; Sahlgren, C.; Lindén, M. *Nanoscale* **2010**, *2*, 1870−1883.
(4) He, Q.; Shi, J. *J. Mater. Chem.* **2011**, *21*, 5845−5855.
(5) Faraji, A. H.; Wipf, P. *Bioorgan. Med. Chem.* **2009**, *17*, 2950−2962.
(6) Zhang, Q.; Liu, F.; Nguyen, K. T.; Ma, X.; Wang, X.; Xing, B.; Zhao, Y. *Adv. Funct. Mater.* **2012**, *22*, 5144−5156.
(7) Chen, C.; Geng, J.; Pu, F.; Yang, X.; Ren, J.; Qu, X. *Angew. Chem., Int. Ed.* **2011**, *50*, 882−886.
(8) Baeza, A.; Guisasola, E.; Ruiz-Hernández, E.; Vallet-Regí, M. *Chem. Mater.* **2012**, *24*, 517−524.
(9) Wang, C.; Li, Z.; Cao, D.; Zhao, Y.-L.; Gaines, J. W.; Bozdemir, O. A.; Ambrogio, M. W.; Frasconi, M.; Botros, Y. Y.; Zink, J. I.; Stoddart, J. F. *Angew. Chem., Int. Ed.* **2012**, *51*, 5460−5465.
(10) Lee, J.; Park, J.; Singha, K.; Kim, W. J. *Chem. Commun.* **2013**, *49*, 1545−1547.
(11) Lim, J.-S.; Lee, K.; Choi, J.-N.; Hwang, Y.-K.; Yun, M.-Y.; Kim, H.-J.; Won, Y. S.; Kim, S.-J.; Kwon, H.; Huh, S. *Nanotechnolgy* **2012**, *23*, 085101.
(12) Hwang, Y.-K.; Choi, J.-N.; Cho, J.-H.; Kwon, H.; Huh, S. *Eur. J. Inorg. Chem.* **2012**, 3379−3383.
(13) Beck, J. S.; Vartuli, J. C.; Roth, W. J.; Leonowicz, M. E.; Kresge, C. T.; Schmitt, K. D.; Chu, C. T. W.; Olson, D. H.; Sheppard, E. W.; McCullen, S. B.; Higgins, J. B.; Schlenker, J. L. *J. Am. Chem. Soc.* **1992**, *114*, 10834−10843.
(14) Zhao, D.; Feng, J.; Huo, Q.; Melosh, N.; Fredrickson, G. H.; Chmelka, B. F.; Stucky, G. D. *Science* **1998**, *279*, 548−552.
(15) Zhao, D.; Huo, Q.; Feng, J.; Chmelka, B. F.; Stucky, G. D. *J. Am. Chem. Soc.* **1998**, *120*, 6024−6036.
(16) Kim, M.-H.; Na, H.-K.; Kim, Y.-K.; Ryoo, S.-R.; Cho, H. S.; Lee, K. E.; Jeon, H.; Ryoo, R.; Min, D.-H. *ACS Nano* **2011**, *5*, 3568−3576.
(17) Na, H.-K.; Kim, M.-H.; Park, K.; Ryoo, S.-R.; Lee, K. E.; Jeon, H.; Ryoo, R.; Hyeon, C.; Min, D.-H. *Small* **2012**, *8*, 1752−1761.
(18) Na, K.; Choi, M.; Ryoo, R. *Microporous Mesoporous Mater.* **2013**, *166*, 3−19.
(19) Janssen, A. H.; Koster, A. J.; de Jong, K. P. *J. Phys. Chem. B* **2002**, *106*, 11905−11909.
(20) de Jong, K. P.; Zečević, J.; Friedrich, H.; de Jongh, P. E.; Bulut, M.; van Donk, S.; Kenmogne, R.; Finiels, A.; Hulea, V.; Fajula, F. *Angew. Chem., Int. Ed.* **2010**, *49*, 10074−10078.
(21) Huh, S.; Wiench, J. W.; Yoo, J.-C.; Pruski, M.; Lin, V. S.-Y. *Chem. Mater.* **2003**, *15*, 4247−4256.
(22) Huh, S.; Wiench, J. W.; Trewyn, B. G.; Song, S.; Pruski, M.; Lin, V. S.-Y. *Chem. Commun.* **2003**, 2364−2365.
(23) Yu, J.; Shi, J.-L.; Chen, H.-R.; Yan, J.-N.; Yan, D.-S. *Microporous Mesoporous Mater.* **2001**, *46*, 153−162.
(24) Huh, S.; Chen, H.-T.; Wiench, J. W.; Pruski, M.; Lin, V. S.-Y. *J. Am. Chem. Soc.* **2004**, *126*, 1010−1011.
(25) Huh, S.; Chen, H.-T.; Wiench, J. W.; Pruski, M.; Lin, V. S.-Y. *Angew. Chem., Int. Ed.* **2005**, *44*, 1826−1830.
(26) Meng, Q.; Xiang, S.; Zhang, K.; Wang, M.; Bu, X.; Xue, P.; Liu, L.; Sun, H.; Yang, B. *J. Colloid Interf. Sci.* **2012**, *384*, 22−28.
(27) Valle-Vigón, P.; Sevilla, M.; Fuertes, A. B. *Mater. Lett.* **2010**, *64*, 1587−1590.
(28) Zhang, Q.; Zhang, T.; Ge, J.; Yin, Y. *Nano Lett.* **2008**, *8*, 2867−2871.
(29) Asefa, T.; Shi, Y.-L. *J. Mater. Chem.* **2008**, *18*, 5604−5614.
(30) Slowing, I. I.; Trewyn, B. G.; Lin, V. S.-Y. *J. Am. Chem. Soc.* **2006**, *128*, 14792−14793.
(31) Połtowicz, J.; Serwicka, E. M.; Bastardo-Gonzalez, E.; Jones, W.; Mokaya, R. *Appl. Catal., A* **2001**, *218*, 211−217.
(32) Figueira, F.; Cavaleiro, J. A. S.; Tomé, J. P. C. *J. Porphyrins Phthalocyanines* **2011**, *15*, 517−533.
(33) Ethirajan, M.; Chen, Y.; Joshi, P.; Pandey, R. K. *Chem. Soc. Rev.* **2011**, *40*, 340−362.
(34) Yoshida, A.; Kakegawa, N.; Ogawa, M. *Res. Chem. Intermed.* **2003**, *29*, 721−731.
(35) Huang, X.; Meng, X.; Tang, F.; Li, L.; Chen, D.; Liu, H.; Zhang, Y.; Ren, J. *Nanotechnolgy* **2008**, *19*, 445101.
(36) Yasutaka, K.; Takato, Y.; Takashi, K.; Kohsuke, M.; Hiromi, Y. *J. Phys. Chem. B* **2011**, *115*, 10335−10345.